Journal of Experimental Nanoscience
Publication details, including instructions for authors and subscription information:
http://www.informaworld.com/smpp/title~content=t716100757

Ultrasonic-assisted synthesis of $Ca(OH)_2$ and CaO nanostructures

Mohammad Amin Alavi[a]; Ali Morsali[a]
[a] Department of Chemistry, Faculty of Sciences, Tarbiat Modares University, Tehran, Islamic Republic of Iran

Online publication date: 24 March 2010

To cite this Article Amin Alavi, Mohammad and Morsali, Ali(2010) 'Ultrasonic-assisted synthesis of $Ca(OH)_2$ and CaO nanostructures', Journal of Experimental Nanoscience, 5: 2, 93 — 105
To link to this Article: DOI: 10.1080/17458080903305616
URL: http://dx.doi.org/10.1080/17458080903305616

Journal of Experimental Nanoscience
Vol. 5, No. 2, April 2010, 93–105

Taylor & Francis
Taylor & Francis Group

Ultrasonic-assisted synthesis of $Ca(OH)_2$ and CaO nanostructures

Mohammad Amin Alavi and Ali Morsali*

Department of Chemistry, Faculty of Sciences, Tarbiat Modares University, P.O. Box 14155-4838, Tehran, Islamic Republic of Iran

(*Received 5 May 2009; final version received 25 August 2009*)

Calcium hydroxide nanostructures have been synthesised by the reaction of calcium acetate with sodium hydroxide or tetramethylammonium hydroxide by a sonochemical method. Reaction conditions, such as the concentration of the Ca^{2+} ion, ageing time and power of the ultrasonic device show important roles in the size, morphology and growth process of the final products. The calcium oxide nanoparticles have been obtained by heating of calcium hydroxide nanostructures at 600°C. The calcium hydroxide and calcium oxide nanostructures were characterised by transmission electron microscopy, scanning electron microscopy and X-ray powder diffraction.

Keywords: $Ca(OH)_2$; CaO; nanostructure; powder diffraction; thermogravimetric analysis; electron microscopy

1. Introduction

Inorganic materials are of fundamental interest and technological importance due to their broad application in materials chemistry. It is well documented that the properties of inorganic nanomaterials depend greatly on their morphologies. Thus, the design and controlled synthesis of nanostructures with different morphological configurations and size distribution on a large scale is very important from the viewpoint of both basic science and technology [1–4]. CaO is a material having a wide range of applications, being of continuous interest in the field of materials research. Pure CaO is an oxide with cubic lattice structure [5] with anisotropic catalytic properties and is often investigated as a component in catalytic powder materials or cements [6]. CaO can also be used as a component of composite or doped material, while the application fields become extended by the thin film technology due to the possibility to modify electrical and optical (dielectric) properties. For instance, ZrO_2–CaO crystals have been studied for the application as planar waveguides [7], and calciumaluminate glasses for a variety of applications, such as laser windows and fibre optics [8]. Advanced sensor properties in tin oxide films have been obtained with the aid of CaO doping [9]. CaO is also known as a dopant able to stabilise cubic zirconia [10] or hafnia [11], and fluently modify the refractive index of silicate glasses [12]. Due to its wide band gap (7.1 eV) [13], high dielectric constant

*Corresponding author. Email: morsali_a@yahoo.com

ISSN 1745–8080 print/ISSN 1745–8099 online

DOI: 10.1080/17458080903305616
http://www.informaworld.com

(11.8) [14] and ability to form solid solutions and ternary crystalline phases CaO and their ternary alloys can be considered as interesting dielectric gate materials, exhibiting high mechanical and radiation resistance [15]. Although pure CaO cannot be regarded as a stable compound in air because of its ability to form hydroxides, or at least accommodate hydrogen as substitutional defects, [16] different methods are being considered for the preparation of CaO films on silicon [16,17] but the classic route for CaO production involves thermal treatment of $CaCO_3$ [18] and also the CaO produced after this treatment hydrated (slaked) to produce $Ca(OH)_2$ [19]. The effects of additives on the formation of high surface area, nanocrystalline $Ca(OH)_2$ have been studied too [20] and so the hydrate can afterwards be dehydroxilated via thermal treatment, yielding a highly reactive, nanocrystalline CaO [21]. Sonochemistry is the research area in which molecules undergo a chemical reaction due to the application of powerful ultrasound radiation (20 KHz–10 MHz) [22]. In recent years many kinds of nanomaterials have been prepared by this method. The nanomaterials whose syntheses were reported are ZnS [23,24], Sb_2S_3 [25,26], HgSe [27], SnS_2 [28], CdS [29], CdSe [29], PbE (E = S, Se, Te) [30], CuS [31], Ag_2Se [32], MnO_2 [33], $CdCO_3$ [34], $BaCO_3$ [35], Co_3O_4 [36] and Mn_3O_4 [36]. In the present work we have developed a simple sonochemical [37] method to prepare CaO nanoparticles, wherein calcium hydroxide is synthesised as a precursor compound by the reaction of calcium acetate and sodium hydroxide (NaOH) in an ultrasonic device and is converted to CaO by heating at 600°C in a furnace. The $Ca(OH)_2$ and CaO nanostructures have been characterised by X-ray powder diffraction (XRD) and also the morphology and size of the nanostructures have been observed by transmission electron microscopy (TEM) and scanning electron microscopy (SEM). The reactions have been done in several conditions to find out the role of different factors, such as the ageing time of the reaction, power of ultrasound device and the concentration of the Ca^{2+} ion on the size and morphology of the nanostructures.

Comparing with the wet chemical routes, such as hydrothermal or solvothermal methods this sonochemical method does not require pressure controlling and high temperature. Comparing with template-assisted method that requires surfactant and pH value controlling, this procedure does not need any surfactant and control of pH values. There are several reports about the synthesis of CaO nanostructures so far. Different methods may still be considered for the preparation of CaO films, such as dehydration of laser-ablated $Ca(OH)_2$ layers [38]. Calcium oxide films have also been obtained by atomic layer deposition (ALD) process from calcium h-diketonate, CO_2 and ozone [17].

2. Experimental

To prepare the $Ca(OH)_2$ precursor different amounts of NaOH or tetramethylammonium hydroxide (TMAH) solutions with concentrations of 0.1 M were added to the 0.1, 0.2, 0.3 M solution of calcium acetate in ethanol. Then the suspension was ultrasonically irradiated with a high-density ultrasonic probe immersed directly into the solution under various conditions (Table 1). A multiwave ultrasonic generator (Sonicator_3000; Misonix, Inc., Farmingdale, NY, USA), equipped with a converter/transducer and titanium oscillator (horn), 12.5 mm in diameter, operating at 20 kHz with a maximum power output of 600 W, was used for the ultrasonic irradiation. The wave amplitude in each experiment

Table 1. Experimental condition for the preparation of $Ca(OH)_2$.

Sample	$Ca(CH_3COO)_2$ (M)	NaOH (0.1 M)	Ageing time	Ultrasound power (W)	Particles size (nm)
1	0.1 (25ml)	50 ml	1 h	30–60	47–95
2	0.2 (25 ml)	100 ml	1 h	30–60	51–87
3	0.3 (25 ml)	150 ml	1 h	30–60	61–190
4	0.1 (25 ml)	50 ml	30 min	30–60	80–120
5	0.1 (25 ml)	50 ml	2 h	30–60	43–67
6	0.1 (25 ml)	50 ml	1 h	120–150	72–180
7	0.1 (25 ml)	50 ml	1 h	360–390	85
8	0.1 (50 ml) + 2 g PVA	100 ml	1 h	30–60	43–75
9	0.1 (25 ml)	25 ml TMAH (0.2 M)	1 h	30–60	72–200
10	0.1 (25 ml) + 1 g $NaNO_3$	50 ml	1 h	30–60	130–200

was adjusted as needed. To form the CaO powders the obtained precipitates were heated at 600°C in a furnace. To investigate the role of surfactants on the size and morphology of nanostructures, we used 2 g of polyvinyl alcohol (PVA) in the reaction with optimised conditions. To investigate the role of alkali salts on the morphology of nanostructures, 1 g $NaNO_3$ was added to the solution of precursors in the reaction No. 10.

The XRD measurements were performed using a X'pert diffractometer of Philips company with monochromatised Cuk_α radiation. The crystallite sizes of selected samples were estimated using the Scherrer method. The samples were characterised with TEM (Philips CM200 FEG (Field Emission Gun)) and scanning electron microscope (SEM) (Philips XL 30) with gold coating. IR spectra were recorded on a SHIMADZU–IR460 spectrometer in a KBr matrix and BET surface area of the samples was determined from N_2 adsorption–desorption isotherms using a Surface Area Analyzer (BET (Brunauer Emmett Teller), BELSORP mini-II).

3. Results and discussion

Scheme 1 shows the reaction between calcium acetate and sodium hydroxide to prepare calcium hydroxide and calcium oxide.

Figure 1(a) shows the XRD pattern of a typical sample of $Ca(OH)_2$ (sample No. 1) prepared by the sonochemical process in ethanol and Figure 1(b) shows the XRD pattern of the above samples after heating at 600°C. The patterns match with the standard patterns of $Ca(OH)_2$ and CaO. The crystalline phases of $Ca(OH)_2$ and CaO are hexagonal and cubic, space groups $P3m1$ and $Fm3m$ with the lattice parameters $a = 3.5899$ Å, $c = 4.916$ Å, $z = 1$ and $a = 4.81059$ Å, $z = 4$ for $Ca(OH)_2$ and CaO, respectively, which are close to the reported values, (JCPDS cards number 44-1481 and 37-1497). The sharp diffraction peaks of the sample indicated that well-crystallised CaO crystals can be easily obtained under current synthetic conditions. No characteristic peaks of other impurities have been detected, which indicated that the products are of high purity. The broadening of the peaks indicated that the particles were of nanometre scale. Estimated from the Scherrer formula, $D = 0.891\lambda/\beta\cos\theta$, where D is the average crystallite size, λ is the X-ray wavelength (0.15405 nm), and θ and β are the diffraction angle and full-width at half maximum of an observed peak, respectively [39], the average crystallite size of the particles

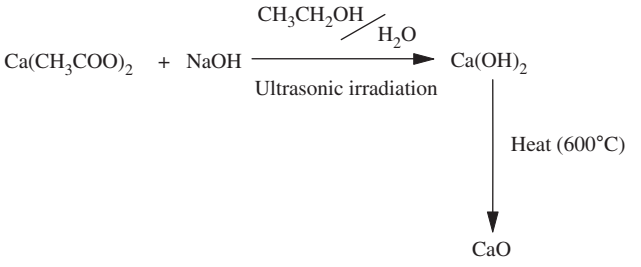

Scheme 1. The mechanism of CaO formation.

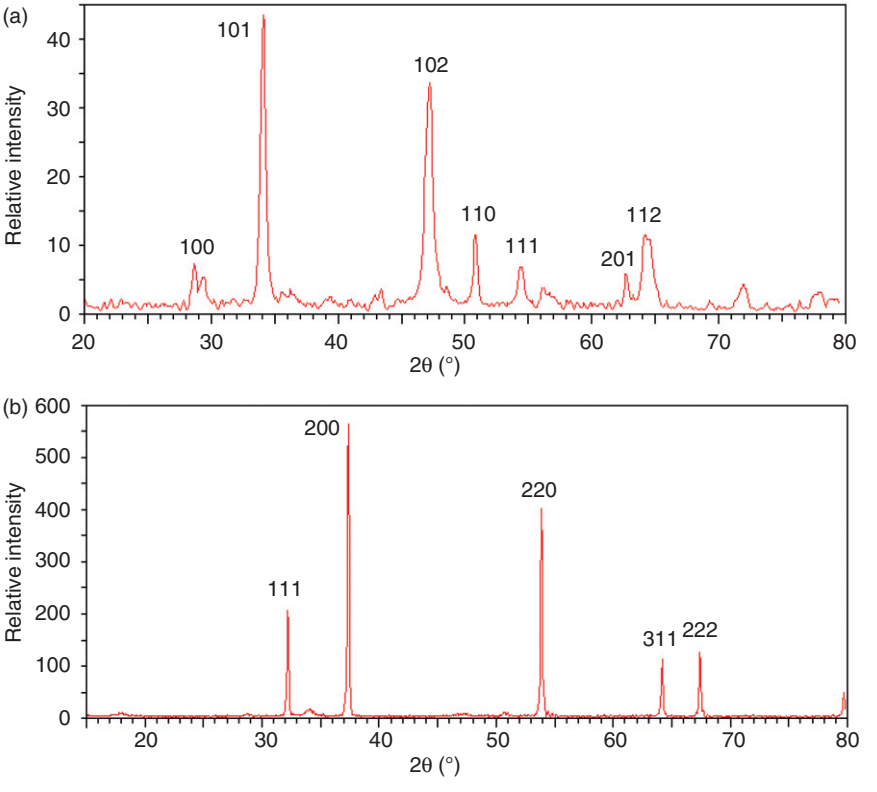

Figure 1. The XRD patterns of (a) $Ca(OH)_2$ and (b) CaO nanoparticles (sample No. 1).

of sample No. 1 ($Ca(OH)_2$ particles) is 43.5 nm and for above sample after heating at 600°C (CaO particles) is 98.6 nm.

The morphology, structure and size of the samples are investigated by an SEM. The effect of various parameters on the size and morphology of nanostructures was investigated.

(1) The concentration of the Ca^{2+} ion: Figure 2(a) indicates the original morphology of the particles of sample No. 1 with the diameters varying between 20 and 100 nm.

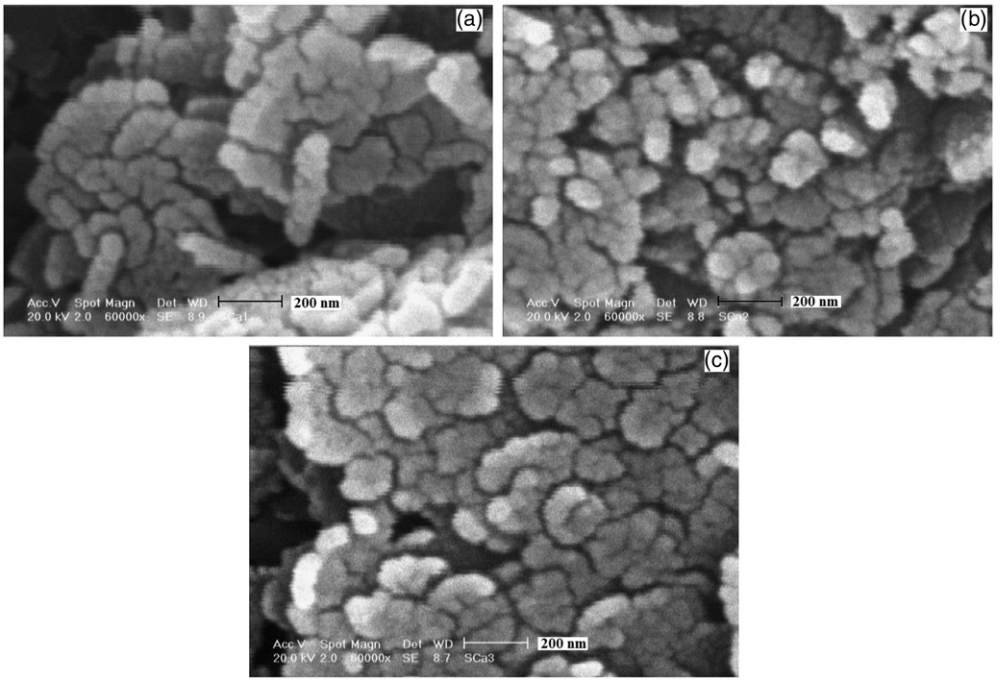

Figure 2. SEM images of $Ca(OH)_2$ nanostructures (various concentrations of Ca^{2+} ion): (a) sample No. 1 (0.1 M), (b) sample No. 2 (0.2 M) and (c) sample No. 3 (0.3 M) (the scale bar is 200 nm).

For investigation of the role of concentration of Ca^{2+} ion in the morphology and size of the particles, the concentration was increased to 0.2 and 0.3 M (sample Nos. 2 and 3). According to Figure 2(b) and (c), the particles obtained from above reactions have larger sizes than the obtained particles of sample No. 1.

(2) Ageing time: For understanding the effect of ageing time on the morphology and size of the particles, the reaction was carried out in 30 min, 1 h and 2 h. Figure 3(a) shows the SEM image of the reaction with the ageing time of 30 min (sample No. 4). As seen from Figure 3(a), with decrease in the ageing time to 30 min, the obtained particles were bigger than the particles of sample No. 1 (with the ageing time 1 h), whereas with increase in the ageing time of reaction to 2 h (sample No. 5) the nanoparticles with 52 nm in diameter were formed (Figure 3b).

(3) Power of ultrasound device: To investigate the role of sonicator device power, the reaction was carried out in three various powers (sample Nos. 1, 6 and 7). Figure 4(a) shows the SEM images of the sample No. 6. As seen, with increasing power (sample No. 6), the size of the particles was decreased, whereas the morphology was not changed (sample No. 7 and Figure 4b). However, as seen in Figure 4(b), the best morphology with smaller particles and good distribution was obtained for the sample No. 7 with the concentration of Ca^{2+} ion of 0.1 M, ageing time of 1 h and the ultrasound device power of 360 W.

Figure 5(a) shows the SEM image of the sample No. 8 and the role of PVA on the morphology of this sample is obvious. It has been reported that the presence of a capping

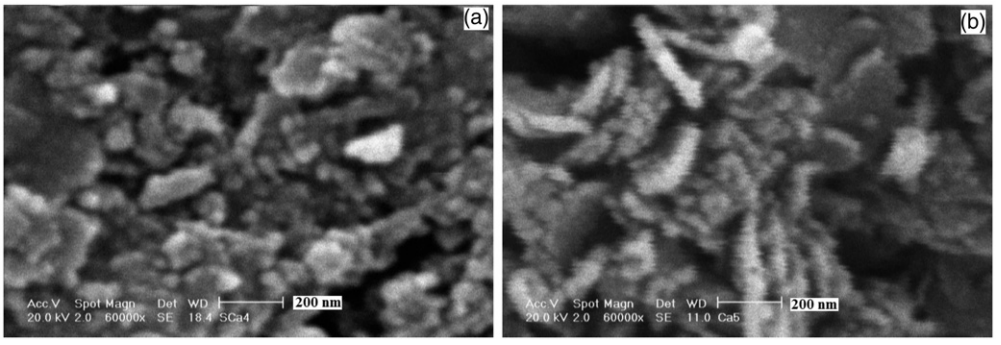

Figure 3. SEM images of $Ca(OH)_2$ nanostructures (various ageing times): (a) sample No. 4 (30 min) and (b) sample No. 5 (2 h) (the scale bar is 200 nm).

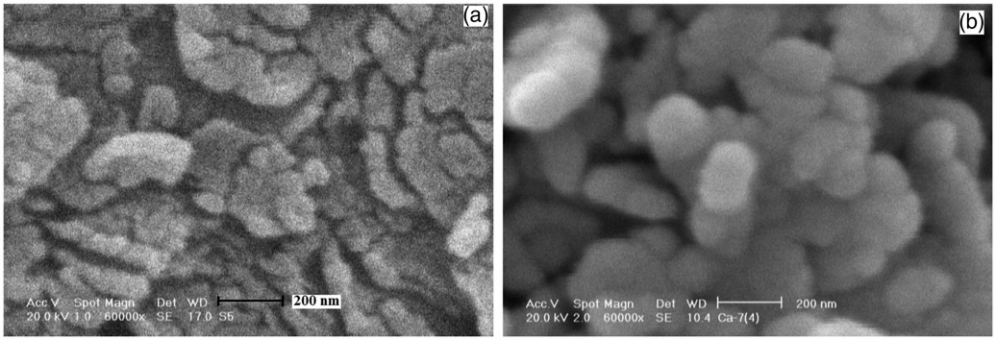

Figure 4. SEM images of $Ca(OH)_2$ nanostructures (various ultrasonic device power): (a) sample No. 6 (120–150 W) and (b) sample No. 7 (360–390 W) (the scale bar is 200 nm).

molecule (such as PVA) can alter the surface energy of crystallographic surfaces, in order to promote the anisotropic growth of the nanocrystals [40,41]. In this work, PVA adsorbs on the crystal nuclei and it helps the $Ca(OH)_2$ nanoparticles to grow separately. The TMAH as a weaker base was used for the reaction at optimised condition. As seen in Figure 5(b) (sample No. 9) TMAH has no effect on the morphology of obtained nanostructures. Alkali salts have been used in many procedures of synthesising nanostructures to change the morphology and to convert the nanoparticles to one dimensional structure, such as nanorods or nanowires and to design advanced materials with anisotropic properties [42]. To investigate the role of alkali salts on the morphology of $Ca(OH)_2$ nanostructures the reactions were performed in the presence of sodium nitrate. As shown in Figure 5(c) (sample No. 10) the nanoparticles grew separately and the one-dimensional nanostructures with suitable lengths are obtained.

The reaction was done without sonication for investigating the role of sonication on the morphology of product, as seen in Figure 6(a), the particles are not at nanosizes. For further investigation, the reaction in optimised conditions was done in the presence of PVA without sonication for investigating the effect of a stabiliser on the morphology

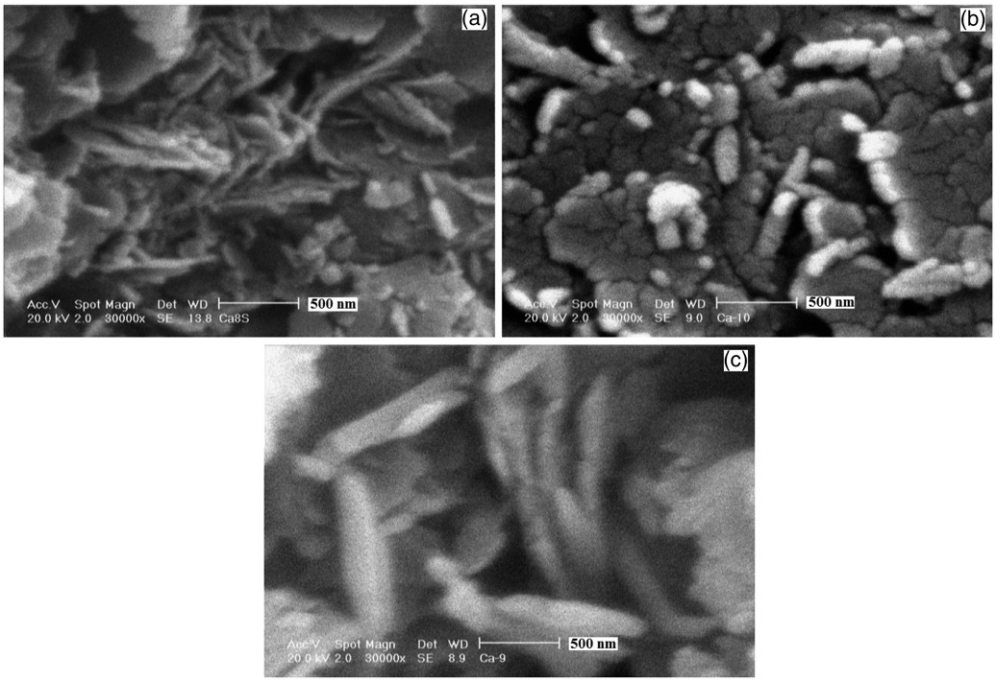

Figure 5. SEM images of $Ca(OH)_2$ nanostructures: (a) sample No. 8, (b) sample No. 9 and (c) sample No. 10 (the scale bar is 500 nm).

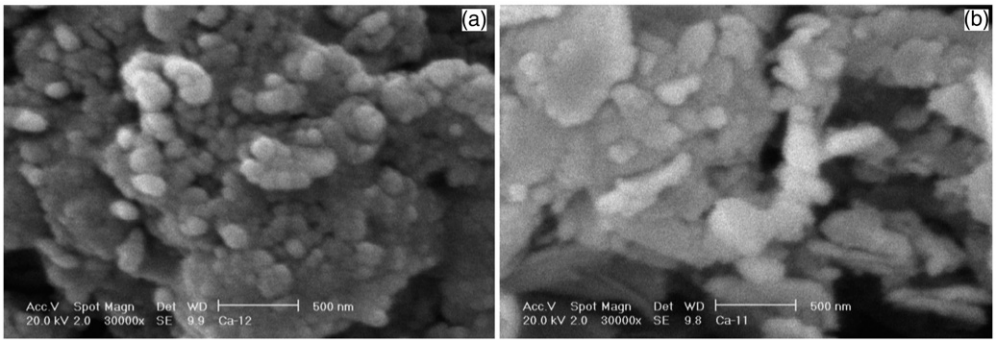

Figure 6. SEM images of $Ca(OH)_2$: (a) without sonication and (b) in the presence of PVA without sonication (the scale bar is 500 nm).

of the product. Comparing the result of this reaction (Figure 6b) with Figure 5(a), PVA has no effect on the particles growth in the absence of sonication.

SEM images of CaO particles are illustrated in Figure 7(a)–(e) for sample Nos. 1, 7, 5, 6 and 9, respectively. Comparison of the SEM images shows that the smallest and the spherical CaO particles with good separation were obtained for sample No. 7 (Figure 7b).

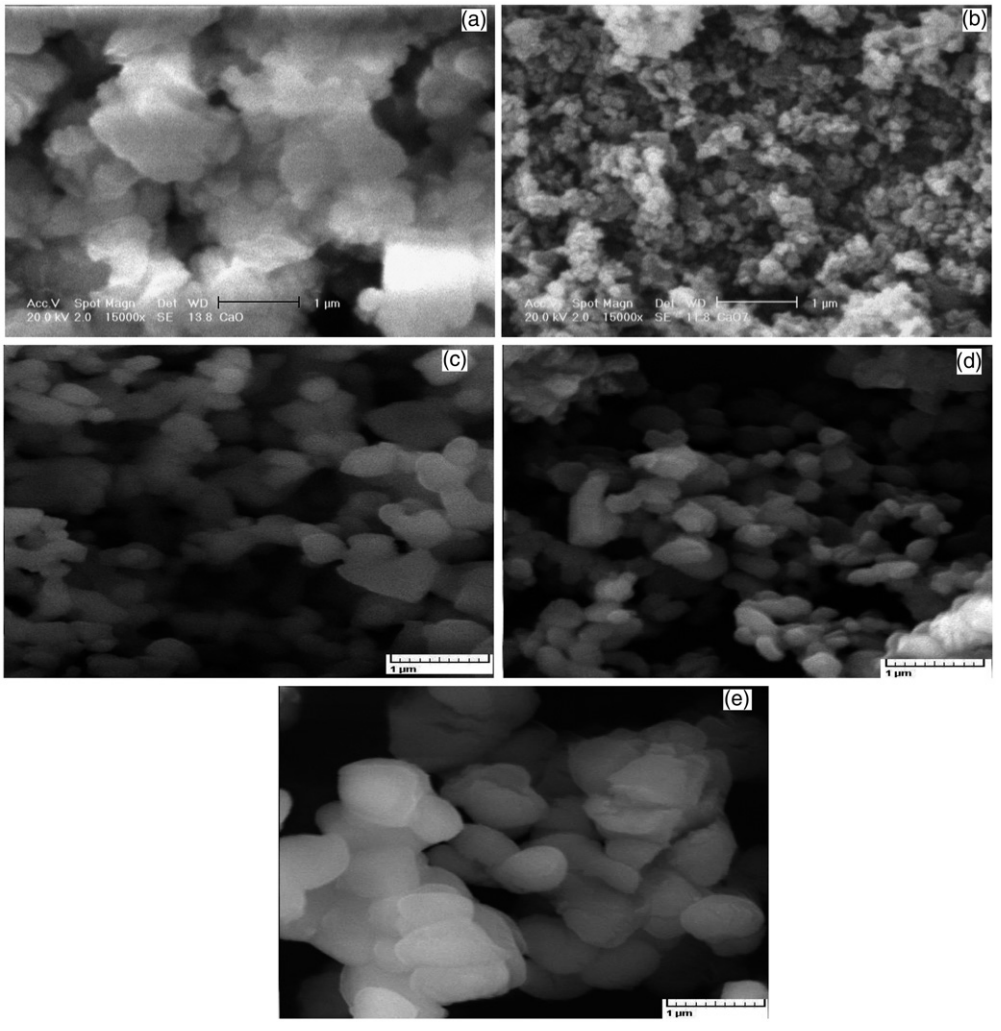

Figure 7. SEM images of CaO nanoparticles: (a) sample No. 1, (b) sample No. 7, (c) sample No. 5, (d) sample No. 6 and (e) sample No. 9 (the scale bar is 1 µm).

Figure 8 shows the XRD patterns of sample No. 7 and sample No. 9 before ($Ca(OH)_2$ nanostructures) and after calcination (CaO nanoparticles), respectively. The estimation from the Scherrer formula shows that the average crystallite size for samples of $Ca(OH)_2$ 7, $Ca(OH)_2$ 9, CaO 7 and CaO 9 are 43.97, 35.34, 77.7 and 124.69 nm, respectively. The crystallite size of the sample No. 9 nanostructures are smaller than sample No. 7, whereas after calcination, the crystallite size of CaO particles of sample No. 7 is smaller than sample No. 9 and these results confirm that the solid state transformation of $Ca(OH)_2$ to CaO particles in this current condition is topotactic as described in reported papers [43,44].

TEM images and the ED pattern of $Ca(OH)_2$ nanoparticles (sample No. 1) are illustrated in Figure 9. As seen from the SEM images of sample No. 1, it was thought that

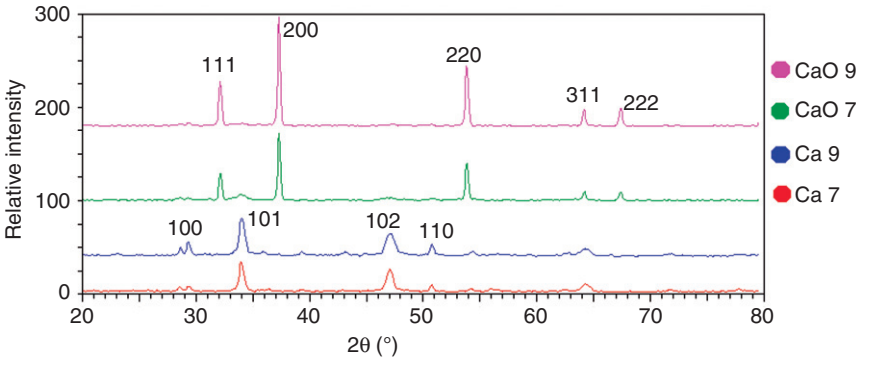

Figure 8. The XRD patterns of sample No. 7 and sample No. 9 for $Ca(OH)_2$ (marked as Ca) and CaO nanostructures.

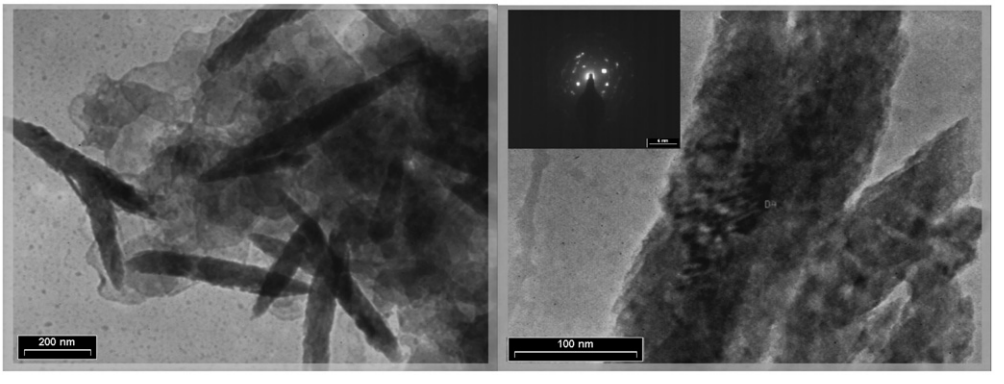

Figure 9. TEM images and ED pattern (inset) of $Ca(OH)_2$ (sample No. 1) nanostructures.

the samples are nanorod structures but the real structure that was shown by TEM images (Figure 9) is aggregates of nanoparticles.

To investigate the size distribution of the nanoparticles a particle size histogram was prepared for sample No. 7 after heating at 600°C, (Figure 10). Most of the particles possess sizes in range from 65 to 80 nm.

BET surface area measurements were performed on the three samples, sample without sonication (as marked $Ca(OH)_2$ (WU)), sample No. 7 (as marked $Ca(OH)_2$-7) and sample No. 7 after calcination at 600°C (as marked CaO-7) and all the results are provided in Table 2. Also the mean pore diameters were calculated. Without sonication the measured surface area was less than the same sample (sample No. 7) in the presence of ultrasonic irradiation, but after calcination the measured surface area decreased to 8.89 m^2/g for CaO nanoparticles that is comparable with surface area of CaO produced in some other reported methods [45].

The sonochemical method comparing with the other methods which have been used for preparing the CaO nanostructures [16,17] is very fast and it does not need high

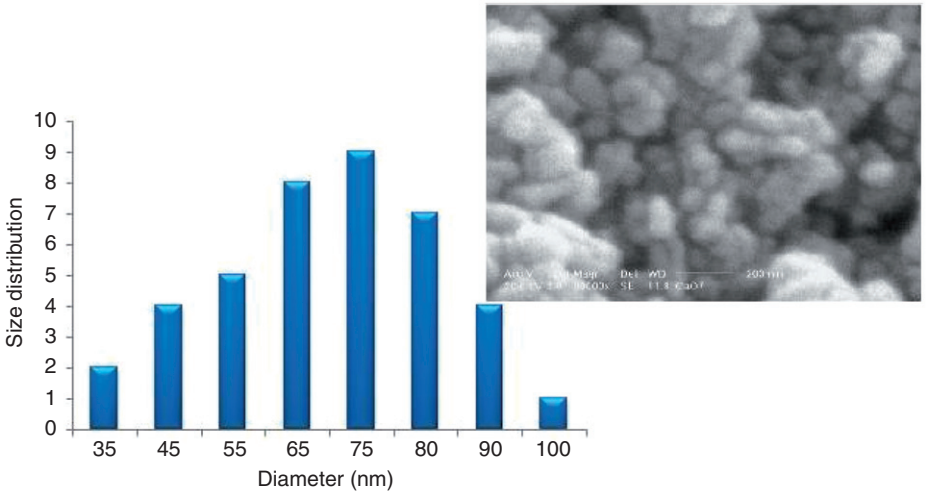

Figure 10. Particle size histogram and SEM images (inset) of CaO (sample No. 7).

Table 2. BET surface area values and mean pore diameters.

Sample	Surface area (m^2/g)	Mean pore diameter (nm)
$Ca(OH)_2$ (WU)	17.45	2.26
$Ca(OH)_2$-7	31.45	2.293
CaO-7	8.89	2.291

Note: WU = without sonication.

temperatures during the reactions, using the surfactants is not necessary for this method and the other advantage of using ultrasound radiation is that it yields smaller particles [46]. The effects of ultrasound radiation on chemical reactions are due to the very high temperatures and pressures that develop during the sonochemical cavity collapse by acoustic cavitation. There are two regions of sonochemical activity, as postulated by Suslick et al. [47,48], the inside of the collapsing bubble, and the interface between the bubble and the liquid, which extends to about 200 nm from the bubble surface. If the reaction takes place inside the collapsing bubble, as is the case for transition metal carbonyls in organic solvents, the temperature inside the cavitation bubble can be from 5100 to 2300 K depending on the vapour pressure of the solvent [47]. If water is used as the solvent, the maximum bubble core temperature that can be attained is close to 4000 K [49]. The product obtained in this case will be amorphous as a result of the high cooling rates ($>10^{10}$ K/s) reached during collapse. On the other hand, if the reaction takes place at the interface, where the temperature has been measured to be 1900 K [47], one expects to get nanocrystalline products. If the solute is ionic, and hence has a low vapour pressure, then during sonication the amount of the ionic species will be very low inside the bubble and

little product is expected to occur inside the bubbles [50]. Since in the present study the solute is ionic, and we get nanocrystalline calcium hydroxide particles, we propose that the formation of the hydroxide particles occurs at the interface between the bubble and the liquid and the ultrasound accelerated the formation of $Ca(OH)_2$.

4. Conclusion

We have successfully synthesised nanocrystalline $Ca(OH)_2$ and CaO through a sonochemical reaction between different concentrations of calcium acetate with sodium hydroxide or TMAH with different ageing times and different sonicated powers. In similar studies, $CdCO_3$ [34], $BaCO_3$ [35], Mn_3O_4 and Co_3O_4 nanostructures [36] were obtained from reaction of $Cd(CH_3COO)_2$, $Ba(CH_3COO)_2$, $Mn(CH_3COO)_2$ and $Co(CH_3COO)_2$ with TMAH or NaOH under ultrasonic condition. The reactions proceeded under ultrasonic conditions resulting in spherical and uniform CaO and $Ca(OH)_2$ nanocrystallites as shown by TEM and SEM observations. The recrystallisation of CaO from $Ca(OH)_2$ was observed at 512°C in air. By heating $Ca(OH)_2$ at 600°C the CaO nanopowders were obtained and the XRD phase analysis showed the formation of CaO with the cubic symmetry. To our best knowledge, this method is the first one for syntheses of nanoparticles of $Ca(OH)_2$ from $Ca(CH_3COO)_2$ by a sonochemical method. This method can be easily controlled and is expected to be applicable to the fabrication of other nanosized particles.

Acknowledgement

Support of this investigation by Tarbiat Modares University and Materials & Energy Research center is gratefully acknowledged.

References

[1] H.T. Shi, L.M. Qi, J.M. Ma, and H.M. Cheng, *Polymer-directed synthesis of penniform $BaWO_4$ nanostructures in reverse micelles*, J. Amer. Chem. Soc. 125 (2003), pp. 3450–3451.

[2] H. Zhang, D.R. Yang, D.S. Li, X.Y. Ma, S.Z. Li, and D.L. Que, *Controllable growth of ZnO microcrystals by a capping-molecule-assisted hydrothermal process*, Cryst. Growth Des. 5 (2005), pp. 547–550.

[3] D.B. Kuang, A.W. Xu, Y.P. Fang, H.Q. Liu, C. Frommen, and D. Fenske, *Surfactant-assisted growth of novel PbS dendritic nanostructures via facile hydrothermal process*, Adv. Mater. 15 (2003), pp. 1747–1750.

[4] F. Kim, S. Connor, H. Song, T. Kuykendall, and P.D. Yang, *Platonic gold nanocrystals*, Angew. Chem. Int. ed. 43 (2004), pp. 3673–3677.

[5] N.H. de Leeuw and J.A. Burton, *Density-functional theory calculations of the interaction of protons and water with low-coordinated surface sites of calcium oxide*, Phys. Rev. B 63 (2001), p. 195417.

[6] D. Kulkarni and I.E. Wachs, *Isopropanol oxidation by pure metal oxide catalysts: Number of active surface sites and turnover frequencies*, Appl. Catal. A 237 (2002), pp. 121–137.

[7] R.I. Merino, J.A. Pardo, J.I. Pena, G.F. de la Fuente, A. Larrea, and V.M. Orera, *Luminescence properties of ZrO_2-CaO eutectic crystals with ordered lamellar microstructure activated with Er^{3+} ions*, Phys. Rev. B 56 (1997), pp. 10907–10915.

[8] L.-G. Hwa, C.-C. Chen, and S.-L. Hwang, *Optical properties of calcium-aluminate oxide glasses*, Chin. J. Phys. 35 (1997), pp. 78–89.
[9] L. Promsong and M. Sriyudthsak, *Thin tin-oxide film alcohol-gas sensor*, Sensors Actuators B, Chem. 25 (1995), pp. 504–506.
[10] M. Boulouz, L. Martin, A. Boulouz, and A. Boyer, *Effect of the dopant content on the physical properties of Y_2O_3–ZrO_2 and CaO–ZrO_2 thin films produced by evaporation and sputtering techniques*, Mater. Sci. Eng. B, Solid-State Mater. Adv. Technol. 67 (1999), pp. 122–131.
[11] C.E. Curtis, L.M. Doney, and J.R. Johnson, *Some properties of hafnium oxide, hafnium silicate, calcium hafnate, and hafnium carbide*, J. Amer. Ceram. Soc. 37 (1954), pp. 458–465.
[12] H. Doweidar, *Refractive index–structure correlations in silicate glasses*, J. Non-Cryst. Solids 277 (2000), pp. 98–105.
[13] R.C. Whited, C.J Flaten, and W.C. Walker, *Exciton thermoreflectance of MgO and CaO*, Solid State Commun. 13 (1973), pp. 1903–1905.
[14] A. Yamasaki and T. Fujiwara, *Electronic structure of the MO oxides ($M = Mg, Ca, Ti, V$) in the GW approximation*, Phys. Rev. B. 66 (2002), pp. 245108–245117.
[15] A.M. Stoneham, *Why model high-k dielectrics?*, J. Non-Cryst. Solids 303 (2002), pp. 114–122.
[16] K. Kukli, M. Ritala, T. Sajavaara, T. Hanninen, and M. Leskela, *Atomic layer deposition of calcium oxide and calcium hafnium oxide films using calcium cyclopentadienyl precursor*, Thin Solid Films. 500 (2006), pp. 322–329.
[17] O. Nilsen, H. Fjellvag, and A. Kjekshus, *Growth of calcium carbonate by the atomic layer chemical vapour deposition technique*, Thin Solid Films. 450 (2004), pp. 240–247.
[18] D. Beruto, A.W. Searcy, and M.G. Kim, *Microstructure, kinetic, structure, thermodynamic analysis for calcite decomposition: Free-surface and powder bed experiments*, Thermochim. Acta 424 (2004), pp. 99–109.
[19] S.S. Potgieter, C.A. Strydom, and O. Gheevarghese, *The effect of ultrasonic energy on lime slaking*, Minerals Eng. 16 (2003), pp. 767–770.
[20] D.L. Moran and M. Rostam-Abadi, Method of preparing hydrated lime (1993) US Patent No. 5223239.
[21] D. Beruto, L. Barco, A. Seary, and G. Spinol, *Characterization of the porous CaO particles formed by decomposition of $CaCO_3$ and $Ca(OH)_2$ in vacuum*, J. Amer. Ceram. Soc. 63 (1980), pp. 439–443.
[22] K.S. Suslick, S.B. Choe, A.A. Cichowlas, and M.W. Grinstaff, *Sonochemical synthesis of amorphous iron*, Nature 353 (1991), pp. 414–416.
[23] M. Sugimoto, *Amorphous characteristics in spinel ferrites containing glassy oxides*, J. Magn. Chem. Mater. 133 (1994), pp. 460–462.
[24] M.V. Landau, L. Vradman, M. Herskowitz, and Y. Koltypin, *Ultrasonically controlled deposition–precipitation: Co-Mo HDS catalysts deposited on wide-pore MCM material*, J. Catal. 201 (2001), pp. 22–36.
[25] H. Wang, Y.N. Lu, J.J. Zhu, and H.Y. Chen, *Sonochemical fabrication and characterization of stibnite nanorods*, Inorg. Chem. 42 (2003), pp. 6404–6411.
[26] J.H. Zhang, Z. Chen, Z.L. Wang, and N.B. Ming, *Sonochemical method for the synthesis of antimony sulfide microcrystallites with controllable morphology*, J. Mater. Res. 18 (2003), pp. 1804–1808.
[27] T. Ding, J.J. Zhu, and J.M. Hong, *Sonochemical preparation of HgSe nanoparticles by using different reductants*, Mater. Lett. 57 (2003), pp. 4445–4449.
[28] H. Mukaibo, A. Yoshizawa, T. Momma, and T. Osaka, *Particle size and performance of SnS_2 anodes for rechargeable lithium batteries*, J. Power Sources 119 (2003), pp. 60–63.
[29] H.L. Li, Y.C. Zhu, S.G. Chen, O. Palchik, J.P. Xlong, Yu. Koltypin, Y. Gofer, and A. Gedanken, *A novel ultrasound-assisted approach to the synthesis of CdSe and CdS nanoparticles*, J. Solid State Chem. 172 (2003), pp. 102–110.

[30] Q. Li, Y. Ding, M.W. Shao, J. Wu, G.H. Yu, and Y.T. Qian, *Sonochemical synthesis of nanocrystalline lead chalcogenides: PbE (E = S, Se, Te)*, Mater. Res. Bull. 38 (2003), pp. 539–543.
[31] X.F. Qiu, J.J. Zhu, and H.Y. Chen, *Controllable synthesis of nanocrystalline gold assembled whiskery structures via sonochemical route*, J. Cryst. Growth 257 (2003), pp. 378–388.
[32] K. Li, X. Liu, H. Wang, and H. Yan, *Rapid synthesis of Ag_2Se nanocrystals by sonochemical reaction*, Mater. Lett. 60 (2006), pp. 3038–3040.
[33] V.G. Kumar and K.B. Kim, *Organized and highly dispersed growth of MnO_2 nano-rods by sonochemical hydrolysis of Mn(3)acetate*, Ultrason. Sonochem. 13 (2006), pp. 549–556.
[34] A. Askarinejad and A. Morsali, *Syntheses and characterization of $CdCO_3$ and CdO nanoparticles by using a sonochemical method*, Mater. Lett. 62 (2008), pp. 478–482.
[35] M.A. Alavi and A. Morsali, *Syntheses of $BaCO_3$ nanostructures by ultrasonic method*, Ultrason. Sonochem. 15 (2008), pp. 833–838.
[36] A. Askarinejad and A. Morsali, *Direct ultrasonic-assisted synthesis of sphere-like nanocrystals of spinel Co_3O_4 and Mn_3O_4*, Ultrason. Sonochem. 16 (2009), pp. 124–131.
[37] J.H. Zhan and X.G. Yang, *Synthesis of nanocrystalline PbSe by sonolysis of $Pb(NO_3)_2$ in non-aqueous solvent*, Inorg. Chem. Commun. 2 (1999), pp. 447–449.
[38] S. Kambe, K. Sato, K. Suezawa, S. Kasuga, S. Ohshima, and K. Okuyama, *Preparation of [111] - oriented CaO film through dehydration of a $Ca(OH)_2$ film*, Mater. Chem. Phys. 54 (1998), pp. 190–193.
[39] J. Yang, C. Lin, and Zh. Wang, *$In(OH)_3$ and In_2O_3 nanorod bundles and spheres: Microemulsion-mediated hydrothermal synthesis and luminescence properties*, J. Lin, Inorg. Chem. 45 (2006), pp. 8973–8979.
[40] W.I. Park, D.H. Kim, S.-W. Jung, and G.-C. Yi, *Metalorganic vapor-phase epitaxial growth of vertically well-aligned ZnO nanorods*, Appl. Phys. Lett. 80 (2002), pp. 4232–4234.
[41] B. Tang, L. Zhuo, J. Ge, J. Niu, and Z. Shi, *Hydrothermal synthesis of ultralong and single-crystalline $Cd(OH)_2$ nanowires using alkali salts as mineralizers*, Inorg. Chem. 44 (2005), pp. 2568–2569.
[42] U. Dahmen, M.G. Kim, and A.W. Searcy, *Microstructural evolution during the decomposition of $Mg(OH)_2$*, Ultramicroscopy 23 (1987), pp. 365–370.
[43] N. Jean-Claude, W. Ginette, and N.H. Brett, *Product crystallite size–reaction rate relationship in $M(OH)_2$–MO decomposition structural transformation mechanism*, J. Chem. Soc. Faraday Trans. 1(74) (1978), pp. 1530–1537.
[44] A. Moira, D. Luigi, G. Rodorico, N. Chiara, and B. Piero, *Colloidal particles of $Ca(OH)_2$: Properties and applications to restoration of frescoes*, Langmuir 17 (2001), pp. 4251–4255.
[45] J. Du, Z. Liu, Y. Huang, Y. Gao, B. Han, W. Li, and G. Yang, *Control of ZnO morphologies via surfactants assisted route in the subcritical water*, J. Cryst. Growth 280 (2005), pp. 126–134.
[46] A. Gedanken, *Using sonochemistry for the fabrication of nanomaterials*, Ultrason. Sonochem. 11 (2004), pp. 47–55.
[47] W.B. McNamara III, Y.T. Didenko, and K.S. Suslick, *Sonoluminescence temperatures during multi-bubble cavitation*, Nature 401 (1999), pp. 772–775.
[48] K.S. Suslick, D.A. Hammerton, and R.E. Cline, *The sonochemical hot spot*, J. Am. Chem. Soc. 108 (1986), pp. 5641–5642; M.W. Grinstaff, A.A. Cichowlas, S.B. Choe, and K.S. Suslick, *Effect of cavitation conditions on amorphous metal synthesis*, Ultrasonics 30 (1992), pp. 168–172.
[49] V. Misik, N. Miyoshi, and P. Riesz, *EPR spin-trapping study of the sonolysis of H_2O/D_2O mixtures: Probing the temperatures of cavitation regions*, J. Phys. Chem. 99 (1995), pp. 3605–3611.
[50] P. Jeevanandam, Yu. Koltypin, O. Palchik, and A. Gedanken, *Synthesis of morphologically controlled lanthanum carbonate particles using ultrasound irradiation*, J. Mater. Chem. 11 (2001), pp. 869–873.